A depth-averaged two-dimensional sediment transport model for environmental studies in the Scheldt Estuary and tidal river network

O. Gourgue[1,2,†], W. Baeyens[3], M. S. Chen[4], A. de Brauwere[1,2,3],
B. de Brye[1,2,‡], E. Deleersnijder[1,5], M. Elskens[3], V. Legat[1,2]

[1] Université catholique de Louvain (UCL)
Institute of Mechanics, Materials and Civil engineering (iMMC)
Avenue Georges Lemaître 4, 1348 Louvain-la-Neuve, Belgium

[2] Université catholique de Louvain (UCL)
Georges Lemaître Centre for Earth and Climate Research (TECLIM)
Chemin du Cyclotron 2, 1348 Louvain-la-Neuve, Belgium

[3] Vrije Universiteit Brussel (VUB)
Laboratory of Analytical and Environmental Chemistry (ANCH)
Pleinlaan 2, 1050 Brussels, Belgium

[4] Vrije Universiteit Brussel (VUB)
Department of Hydrology and Hydraulic Engineering (HYDR)
Pleinlaan 2, 1050 Brussels, Belgium

[5] Université catholique de Louvain (UCL)
Earth and Life Institute (ELI)
Georges Lemaître Centre for Earth and Climate Research (TECLIM)
Chemin du Cyclotron 2, 1348 Louvain-la-Neuve, Belgium

Abstract

This paper presents the sediment module designed for the two-dimensional depth-averaged and one-dimensional section-averaged components of the finite-element model SLIM (Second-generation Louvain-la-Neuve Ice-ocean Model) in the framework of its application to the tidal part of the Scheldt Basin. This sediment transport module focuses on fine-grained, cohesive sediments. It is a necessary tool to undertake environmental biogeochemical studies, in which fine sediment dynamics play a crucial role.

The variables are the suspended sediment concentration (SSC) and the concentration of the sediments freshly deposited on the bottom. Sediment dynamics is controlled by the transport of SSC by advection and diffusion, while deposition and resuspension processes also depend on other physical, chemical and biological conditions . Besides building a functioning fine sediment transport model, the aim of this study is to identify, parametrize

---

[†]Corresponding author; e-mail address: ogourgue@gmail.com
[‡]Now at Free Field Technologies (FFT), Axis Park Louvain-la-Neuve, rue Emile Francqui 1, 1435 Mont-Saint-Guibert, Belgium

and quantify the key processes that are necessary to represent satisfactorily the suspended sediment dynamics in the Scheldt Estuary and tidal river network.

It is known that the settling velocity of suspended sediments is influenced by flocculation. The important factors governing this process include the SSC itself, the turbulence, the shear stress, the salinity, the biological activity and some physicochemical properties (e.g. pH). In this sediment module, only SSC, salinity and biological activity are explicitely taken into account. In addition, the influence of the biological activity on the bottom layer erodibility is considered, as well as the mud proportion on the bottom, because the presence of sand increases the ability of the bottom layer to erode. Finally, the influence of a convergence zone between bottom currents carrying large amounts of fine sediments is also included in the model.

The computer cost of a two-dimensional model is significantly smaller than that of the three-dimensional models traditionally deemed indispensable in sediment transport modeling. Even if the present simplified model is designed for the specific situation of the Scheldt, it produces results that are rather similar to those obtained with more complex, three-dimensional tools, but at a significantly lower cost. Therefore, it is believed that the model presented herein is suitable and useful for long-term environmental simulations in the Scheldt Estuary.

Key words: fine sediments, flocculation, estuary, river, Scheldt, model, depth-averaged, SLIM.

1 Introduction

The Scheldt has its source in France and flows through Belgium and The Netherlands, before discharging into the North Sea near Vlissingen. Its catchment basin is one of the most densely populated in Western Europe (Vanderborght et al., 2007), comprising important cities such as Brussels, Antwerp, Ghent and Lille. In total, more than 10 million inhabitants pour out their wastewater into the Scheldt (Meire et al., 2005), mostly through wastewater treatment plants. Another source of pollution is the considerable and direct supply of toxic non-organic pollutants occurring as a result of the diverse activities by the industrial park around Antwerp (Baeyens et al., 1998b), the second European harbor. Other industrial areas are also concentrated near Lille, the canal from Ghent to Terneuzen, and Vlissingen. Moreover, a significant part of the Scheldt catchment area suffers from a severe agricultural pressure, along with a substantial pesticide contamination (Steen et al., 2001).

Modeling the fine-grained sediment transport processes is a prerequisite for environmental studies. Indeed, the behavior of most biogeochemical

contaminants is closely linked to the dynamics of those sediments. For example, modeling *Escherichia coli* (an indicator for microbiological water quality) without an explicit treatment of the sediment dynamics gives rather good results in the river part of the Scheldt basin (de Brauwere et al., 2011b), but less so in the area of the main estuarine turbidity maximum (ETM). This is supposed to be due to the fact that part of the bacteria are attached to suspended matter and are transported the same way as sediments (Ouattara et al., 2011; de Brauwere et al., 2013). Also, the resuspension of trace metals accumulated in bottom sediments by historical pollution and their dissolution in the water column are generally recognized as a threat to the aquatic environment and ecosystem (Baeyens et al., 1998a). Trace metal modeling with no consideration of sediment dynamics is not even an option. Those two examples illustrate the need for a reliable fine-grained sediment transport model.

The exposure time of a water parcel is the total time it spent in a specific domain, including possible re-entries (de Brye et al., 2012). In the Scheldt Estuary, the maximum exposure time of water is about two to three months (Soetaert and Herman, 1995; Baeyens et al., 1998b; Blaise et al., 2010; de Brauwere et al., 2011a; de Brye et al., 2012). Exposure time of suspended particles is even higher, for they settle and spend considerable time on the bottom (Delhez and Wolk, 2012). Therefore, environmental studies may require relatively long simulations (at least a few months), especially compared to some short-term processes of the sediment dynamics, e.g. tidal induced resuspension and deposition (a few hours). The computer cost for such simulations may be too high when using modern three-dimensional models, but this is less so with one- or two-dimensional models. This points to the need for sufficiently realistic simplified section- or depth-averaged sediment transport models. Moreover, de Brye et al. (2010) showed that the hydrodynamics and the salinity transport in the Scheldt Estuary and tidal river network may be rather well simulated using the combination of a two-dimensional depth-averaged model in the coastal and estuarine areas and a one-dimensional section-averaged model in the river network.

The subject of this paper is the development of a suitable set of equations and parameter values to accurately represent the dynamics of fined-grained sediments in the tidal part of the Scheldt Basin, in the framework of an existing transport model combining two-dimensional depth-averaged and one-dimensional section-averaged equations. The aim is not to build yet another sophisticated sediment transport model such as those of van der Wal et al. (2010) and van Kessel et al. (2011). Instead, the goal is to build a simplified sediment transport model, for the purpose of conducting long-term environmental simulations in the Scheldt Estuary and tidal river network, in order to analyze, in the future, the behavior of biogeochemical pollutants in association with fine-grained sediments in this region.

2 Model domain

The tidal part of the Scheldt Basin may be divided into two subdomains: the estuary, from the mouth to the confluence with the Rupel, and the tidal river network (up to Ghent for the Scheldt River). The model domain is extended downstream to the shelf break (Figure 1). The riverine part, including the tributaries under tidal influence, is simulated resolving one-dimensional section-averaged equations, while the estuarine and marine parts are modeled resolving two-dimensional depth-averaged equations (de Brye et al., 2010).

The Scheldt and its tributaries are rain-fed. The mean discharge rate at Schelle (90 km from the mouth) is about $100\,\mathrm{m^3\,s^{-1}}$ and varies considerably from an average of $60\,\mathrm{m^3\,s^{-1}}$ in summer (with minimal values down to $20\,\mathrm{m^3\,s^{-1}}$) to an average of $180\,\mathrm{m^3\,s^{-1}}$ in winter (and exceptional values up to $600\,\mathrm{m^3\,s^{-1}}$). This phenomenon has a great influence on the transport of dissolved constituants. For example, the location of the transition zone between fresh and salt water is primarily determined by the magnitude of the river discharge (Baeyens et al., 1998b).

The tidal influence is experienced up to Ghent in the Scheldt and in the lower parts of some tributaries. The tidal range is about 4 m at Vlissingen, 5 m at Antwerp, and 2 m at Ghent (where sluices prevent the tide from propagating upstream). However, the tidal action contributes to a lesser degree to the dynamics of dissolved constituants. For example, at a given position, the salinity variation during a tidal period is much smaller than the salinity variation observed during high and low river discharges (Baeyens et al., 1998b). Even though this phenomenon is less marked downstream because the salinity comes closer its marine value, it nevertheless demonstrates the important influence of the upstream flow rate on the transport of dissolved constituants.

In most of the Scheldt Estuary, the observed depth-averaged SSC is about a few $0.01\,\mathrm{kg\,m^{-3}}$. Values may attain $0.5\,\mathrm{kg\,m^{-3}}$ in the area of the most significant ETM around Antwerp. It corresponds more or less to the area between the Belgian-Dutch border and the confluence with the Rupel (Figure 1). This main ETM is primarily due to the large tidal energy occurring in this region (Chen et al., 2005b; Arndt et al., 2007). A second ETM occurs in the tidal river where the SSC may reach $0.3\,\mathrm{kg\,m^{-3}}$ (Chen et al., 2005b). Finally, a third one is located downstream of the mouth. It is marine-dominated and characterized by high wave energy with SSC attaining $0.2\,\mathrm{kg\,m^{-3}}$ (Fettweis and Van den Eynde, 2003; Baeye et al., 2011).

The SSC also undergoes variations at different timescales. The hydrodynamics seems to be directly responsible for the SSC variations observed at the tidal scale (period of a few hours) and at the spring/neap cycle scale (period of a few weeks) because they follow the tidal regime (Chen et al., 2005b; Arndt et al., 2007). In addition, the estuary undergoes seasonal

S1	Terneuzen
S2	Baalhoek
S3	Buoy 87
S4	Buoy 92
S5	Buoy 105
S6	Antwerp
S7	Kruibeke
S8	Bazel
S9	Steendorp
S10	Temse
S11	Mariekerke
S12	Vlassenbroek
S13	Dendermonde
S14	St. Onolfs
S15	Appels
S16	Uitbergen
S17	Wetteren

Table 1: Names of the measurement stations displayed on Figure 1; stations S1 and S2 provide the measurements displayed on Figures 3 to 7; stations S3 to S17 provide the measurements displayed on Figure 9.

variations (the turbidity is two or three higher in winter than in summer) that cannot be explained by the hydrodynamics alone, and that are often associated with variations in water discharge, sediment supply, or biological activity (Fettweis et al., 1998; Chen and Wartel, 2009; van der Wal et al., 2010).

In order to be useful for future environmental studies in the Scheldt Estuary and tidal river network, the following major features of the SSC distribution should be represented accurately:

- the order of magnitude of the SSC throughout the estuary and the tidal river network;

- the variations of the SSC at the tidal, spring/neap cycle and seasonal timescales;

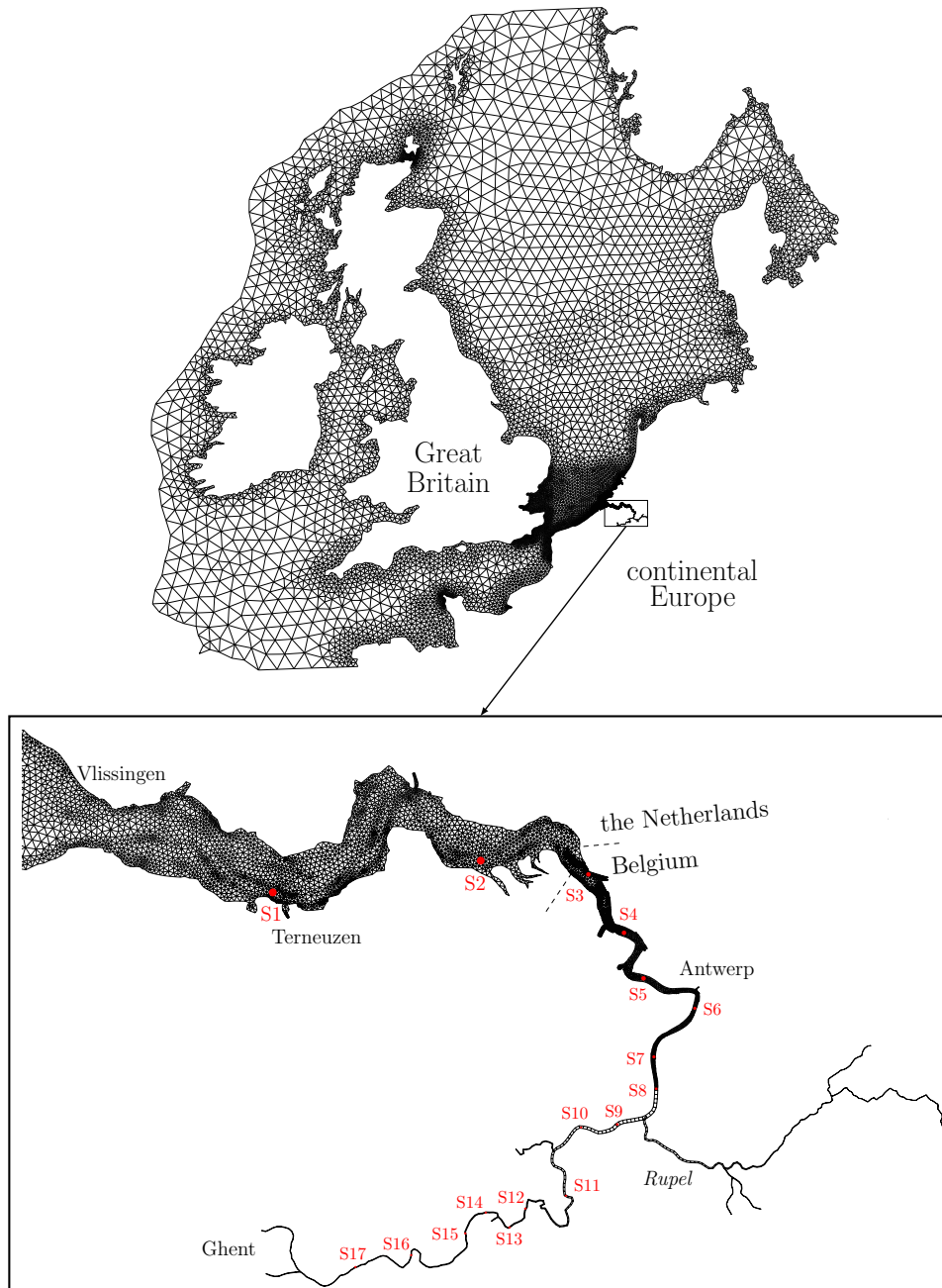- the locations of the main ETM and the river ETM.

Figure 1: Mesh used for the simulations of this study, including the Northwestern European continental shelf, the Scheldt Estuary and the tidal rivers of the Scheldt Basin (about 22000 triangles, and 350 segments in the river part); in red, locations of the measurement stations (Table 1).

3 Model

3.1 Hydrodynamic and salinity modules

The hydrodynamics and salinity transport can be satisfactorily simulated resolving two-dimensional depth-averaged equations in the estuarine part, and one-dimensional section-averaged equations in the riverine part (de Brye et al., 2010). For the sake of simplicity, only the two-dimensional equations are presented here, but their one-dimensional counterparts can be found in Appendix A. The hydrodynamic variables are η [m], the elevation of the water surface above a reference level, and $\boldsymbol{u}$ [m s^{-1}], the depth-averaged horizontal velocity vector. Their evolution is governed by the so-called shallow water equations:

$$\frac{\partial \eta}{\partial t} + \boldsymbol{\nabla} \cdot (H\boldsymbol{u}) \;\; = \;\; 0, \tag{1}$$

$$\frac{\partial \boldsymbol{u}}{\partial t} + \boldsymbol{u} \cdot (\boldsymbol{\nabla} \boldsymbol{u}) + f\boldsymbol{k} \times \boldsymbol{u} \;\; = \;\; -g\boldsymbol{\nabla}\eta - \frac{1}{\rho}\boldsymbol{\nabla}p_{\mathrm{a}}$$
$$+ \frac{1}{H}\boldsymbol{\nabla} \cdot \big(H\nu(\boldsymbol{\nabla}\boldsymbol{u})\big) + \frac{\boldsymbol{\tau}_{\mathrm{s}} - \boldsymbol{\tau}_{\mathrm{b}}}{\rho H}, \tag{2}$$

where t is the time and $\boldsymbol{\nabla}$ the del operator; $H = h + \eta$ is the water depth, with h the reference height of the water column; $f = 2\omega \sin\phi$ is the Coriolis parameter, with ω the angular velocity of the Earth and ϕ the latitude, $\boldsymbol{k}$ is the unit upward vector; g is the gravitational acceleration; ρ is the water density, which is assumed to be constant, in accordance with the Boussinesq approximation, and p_{a} is the atmospheric pressure at the water surface; ν is the horizontal eddy viscosity; $\boldsymbol{\tau}_{\mathrm{s}}$ and $\boldsymbol{\tau}_{\mathrm{b}}$ are the surface and bottom stress vectors, respectively. The depth-averaged salinity S [-] obeys the following transport equation:

$$\frac{\partial(HS)}{\partial t} + \boldsymbol{\nabla} \cdot (H\boldsymbol{u}S) = \boldsymbol{\nabla} \cdot (H\kappa\boldsymbol{\nabla}S), \tag{3}$$

where κ is the diffusivity.

The horizontal eddy viscosity ν is evaluated using the Smagorinsky parametrization (Smagorinsky, 1963). The bottom stress vector is computed using the Chézy-Manning-Strickler formulation:

$$\boldsymbol{\tau}_{\mathrm{b}} = \rho g n^2 \frac{\boldsymbol{u}||\boldsymbol{u}||}{H^{1/3}}, \tag{4}$$

where n is the Manning coefficient, depending on physical properties of the bottom. Its value is calibrated to represent the tide correctly. It is equal to 0.0235 s m$^{-1/3}$ in the continental shelf and increases linearly from the mouth to a value of 0.028 s m$^{-1/3}$ around Antwerp (de Brye et al., 2010). Okubo's formulation (Okubo, 1971) is used to parametrize the diffusivity κ:

$$\kappa = c_\kappa \Delta^{1.15}, \tag{5}$$

where c_κ is a constant and Δ is the characteristic length scale of the mesh (i.e. the longest edge of a triangle in the two-dimensional mesh, or the length of a segment in the one-dimensional mesh). Its value is calibrated to accurately represent the salinity variations in the Scheldt, leading to $c_\kappa = 150 \, \text{m}^{0.85} \, \text{s}^{-1}$. Additional pieces of information about the forcings and parametrizations that are not directly useful for the sediment module may be found in de Brye et al. (2010).

3.2 Sediment module

Three layers are taken into account in the sediment module: the water column where the sediments are in suspension, a layer made up of sediments freshly deposited on the bottom, and a parent layer underneath the latter (Figure 2). Although three layers are considered, the module is only made up of two interacting variables, i.e. C_ss, the depth-averaged concentration of sediments in suspension $[\text{kg} \, \text{m}^{-3}]$, and C_sb, the concentration of bottom sediments in the fresh layer $[\text{kg} \, \text{m}^{-2}]$. The parent layer is an infinite source of sediments that is only eroded when C_sb is locally zero.

While the sediments in suspension are transported by advection and diffusion, those on the bottom are not. In the two-dimensional part of the domain, the suspended sediment concentration and the freshly-deposited sediment concentration obey the following equations:

$$\frac{\partial \big(H C_\text{ss}\big)}{\partial t} + \boldsymbol{\nabla} \cdot \big(H \boldsymbol{u} C_\text{ss}\big) \;\; = \;\; \boldsymbol{\nabla} \cdot \big(H \kappa \boldsymbol{\nabla} C_\text{ss}\big) + E_\text{f} + E_\text{p} - D, \qquad (6)$$

$$\frac{\partial C_\text{sb}}{\partial t} \;\; = \;\; D - E_\text{f}, \qquad (7)$$

where E_f is the erosion rate of sediments from the fresh layer, E_p is the erosion rate of sediments from the parent layer, and D is the deposition rate of sediments on the fresh layer. The equations governing the sediment dynamics in the one-dimensional part of the domain can be found in Appendix A.

In the present version of the sediment module, it is assumed that the parent layer is never supplied and that there is no exchange between the two bottom layers. Moreover, bed-load transport is not taken into account. These assumptions are consistent with the aim of designing a sediment module that is as simple as possible.

The parametrizations of the erosion rates are based on a formula introduced by Partheniades (1965):

$$E_\text{f} \;\; = \;\; \begin{cases} M\left(\dfrac{\tau_\text{b}}{\tau_\text{e}} - 1\right) & \text{if } \tau_\text{b} > \tau_\text{e} \quad \text{and } \; C_\text{sb} > 0, \\[2mm] 0 & \text{otherwise,} \end{cases} \qquad (8)$$

$$E_\text{p} \;\; = \;\; \begin{cases} M\left(\dfrac{\tau_\text{b}}{\tau_\text{e,p}} - 1\right) & \text{if } \tau_\text{b} > \tau_\text{e,p} \quad \text{and } \; C_\text{sb} = 0, \\[2mm] 0 & \text{otherwise.} \end{cases} \qquad (9)$$
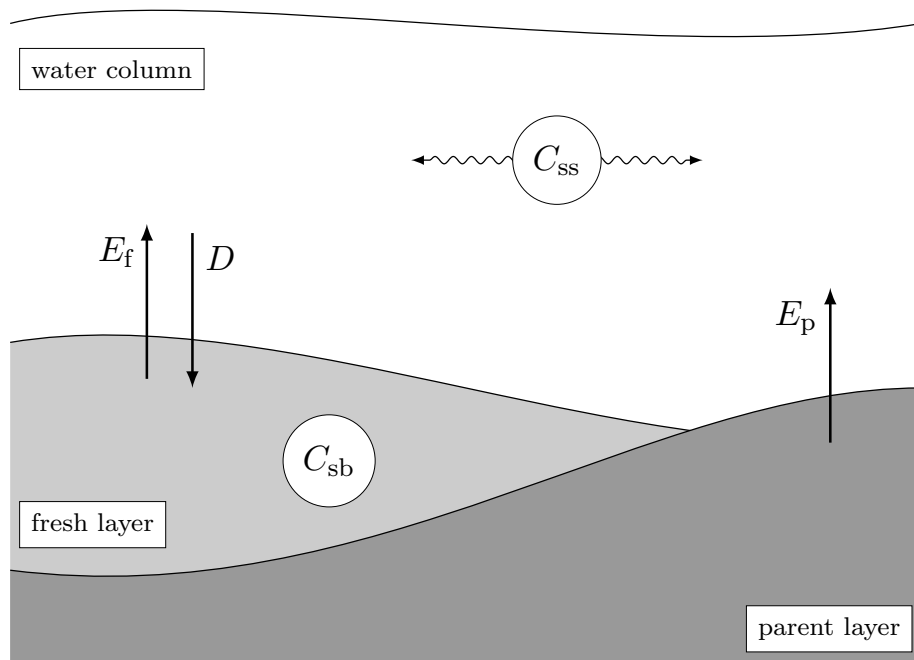
Figure 2: Schematic representation of the sediment module; C_{ss} is the depth-averaged concentration of sediments in suspension and C_{sb} is the concentration of bottom sediments in the fresh layer; E_f is the erosion rate of sediments from the fresh layer, E_p is the erosion rate of sediments from the parent layer, and D is the deposition rate of sediments on the fresh layer.

Sediments are eroded from the fresh layer when τ_b (the norm of the bottom stress vector $\boldsymbol{\tau}_\mathrm{b}$) is higher than a threshold value τ_e, or, if the fresh layer is locally empty, from the parent layer when τ_b is higher than another threshold value $\tau_\mathrm{e,p}$; M is called the erosion rate parameter. The parametrization of the deposition rate is based on a formula introduced by Einstein and Krone (1962):

$$D \;=\; w_\mathrm{s} C_\mathrm{ss}, \tag{10}$$

where w_s is the settling velocity.

As a first attempt, the erosion parameters M, τ_e and $\tau_\mathrm{e,p}$ are considered as constants, with $\tau_\mathrm{e,p} = \tau_\mathrm{e}$. Considering the dynamics of fine-grained sediments, the same hypothesis cannot be made for the settling velocity w_s, which is greatly influenced by flocculation. Flocculation refers to the processes by which suspended sediments aggregate to form flocs, and by which those flocs break up. These processes influence the sediment properties, in particular the settling velocity. The SSC, the turbulence and the shear stress affect the floc growth principally through the increased number of particle collisions per unit of time, while the physicochemical and biological conditions affect the floc growth principally through their effect on the efficiency of the collisions (van Leussen, 1999). The major factors are nevertheless the SSC, the turbulence and the shear stress (Eisma and Kalf, 1979; Winterwerp, 2002; Chen et al., 2005a; Chen, 2009). This is usually taken into account by using the following parametrization of the settling velocity (Dyer, 1989; Wolanski et al., 1992; Berlamont et al., 1993; Wolanski, 1995; Winterwerp, 1998; van Leussen, 1999; Manning et al., 2010; Pejrup and Mikkelsen, 2010):

$$w_\mathrm{s} = w_\mathrm{s,0} \left(\frac{C_\mathrm{ss}}{C_\mathrm{ss,0}} \right)^m, \tag{11}$$

where $C_\mathrm{ss,0} = 0.1\,\mathrm{kg\,m^{-3}}$ is a reference value of the SSC for the Scheldt, $w_\mathrm{s,0}$ is the associated reference settling velocity whose value is determined empirically, and m is a coefficient between 0.5 and 3.5 (van Leussen, 1999). In this case, the turbulence and the shear stress are not taken into consideration explicitly, but the SSC may be seen as a proxy of them (the higher is the turbulence or the shear stress, the higher is the SSC). For want of any empirical estimates of the parameter m in the Scheldt, the value of the latter is arbitrarily taken to be equal to unity. Other values were tested in the framework of this study, but none appeared to lead to a significant improvement of the results. To be complete, it must be emphasized that equation (11) is not valid anymore if SSC is significantly higher than $1\,\mathrm{kg\,m^{-3}}$ (Wolanski et al., 1992; Wolanski, 1995), but it is almost never the case in the Scheldt. Finally, complex flocculation modules (e.g. Baugh and Manning, 2007) can also be coupled to sediment models, but it is not the approach adopted in this project.

When dealing with only one type of sediments, only three parameters must therefore be calibrated: M, τ_e and $w_{s,0}$. If several types of sediments are dealt with, the number of parameters to calibrate is obviously multiplied by the number of sediment types. For the sake of simplicity, only one type is considered in this first study, where the values assigned to the three parameters determine the type of sediments under study. Fine sediments (silt and clay) are considered here because of their importance in the crucial zones like the main ETM and their interaction with contaminants (Baeyens et al., 1998b). In the future, other sediment types may be considered to enrich the module. In the case of non cohesive sediments, however, on top of additional parameters, the use of a proper bedload transport module could probably not be avoided anymore.

3.3 Numerical implementation

Equations (1), (2), (3), (6) and (7) are solved using the finite-element model SLIM[1]. They are discretized on the unstructured mesh displayed in Figure 1, using a discontinuous Galerkin discretization with linear shape functions (P_1^{DG}) for every variable. Doing so, local/global conservation and consistency are warranted for the tracers (White et al., 2008). Stability of the hydrodynamic module is ensured by computing the fluxes at the interface between two triangles using the values deduced from a Roe solver (Comblen et al., 2010). An upwind scheme is used for the tracers. A second-order diagonally implicit Runge-Kutta method is used for the temporal integration (Kärnä et al., 2011), with a time step of 15 minutes. The Scheldt Estuary is characterized by a complex morphology with flood and ebb channels surrounding several large tidal flats and salt marshes. The implicit wetting-drying method used to take this phenomenon into account consists in allowing the sea bed to fluctuate in drying areas, to ensure a positive water thickness at any time (Kärnä et al., 2011).

3.4 Initial and boundary conditions

The initial condition is zero for the variables of the hydrodynamic and sediment modules, and it is based on a long-term averaged profile (Soetaert et al., 2006) for the salinity. Although a regime solution is reached rather quickly (i.e. in less than 5 days for salinity and 10 days for SSC), the simulations start 20 days before the period of interest, so as to make sure that all transients effects associated with the initialization are dissipated. For C_{sb}, it takes longer to reach a regime solution. However, as long as equations (8) and (9) are used with $\tau_e = \tau_{e,p}$, both bottom layers have the same properties and the fresh layer is only useful to keep track of the sediments entered in the domain through the parent layer or the open boundaries. Therefore,

---

[1]Second-generation Louvain-la-Neuve Ice-ocean Model (`www.climate.be/SLIM`)

under these conditions, and as long as the study does not focus specifically on the bottom concentration, a longer initialization period is not needed. A specific study of the bottom concentrations or a more complex version of the module considering different behaviors for the bottom layers would require the simulations to start earlier.

The details about the boundary conditions of the hydrodynamic and salinity modules are found in de Brye et al. (2010), where the ability of SLIM to reproduce the hydrodynamics of the Scheldt and its salinity longitudinal profile is also demonstrated. Upstream boundary conditions of the sediment module are provided by outputs of the Seneque/Riverstrahler model (Thieu et al., 2009). Downstream boundary conditions at the shelf break do not affect the results inside the domain of interest.

4   Results and discussion

As a reminder (Section 2), the objective of this study is to develop a suitable set of equations and parameter values to accurately represent the following features of the SSC in the Scheldt, using SLIM:

- the order of magnitude of the SSC throughout the estuary and the tidal river network;

- the variations of the SSC at the tidal, spring/neap cycle and seasonal timescales;

- the locations of the main ETM and the river ETM.

To that end, the model is first calibrated against time series of turbidity measurements from stations S1 (Terneuzen) and S2 (Baalhoek) in the year 2000. Those measurements were determined optically with MEX3001 turbidity sensors, at different depths (NAP[2] -4 m, -11 m en -17 m in Terneuzen, and NAP -4.5 m en -8 m in Baalhoek). The calibration curves are based on water samples taken at a 4-weekly interval (Villars and Vos, 1999). A spring/summer situation is considered at first, to focus on the tidal and spring/neap cycle scale variations (Section 4.1). New parametrizations of $w_{s,0}$ and τ_e are then defined to deal with the seasonal variations and the model is validated against measurements from the same stations in the year 1999 (Section 4.2). The parametrization of τ_e is refined thereafter to better represent the different behavior of the SSC in Terneuzen and Baalhoek (Section 4.3).

Once the model calibrated and validated for the temporal variations, the parametrization of $w_{s,0}$ is also refined and a new parametrization of M

---

[2]Normaal Amsterdams Peil (NAP) or Amsterdam Ordnance Datum is a vertical datum in use in large parts of Western Europe, though originally created for use in the Netherlands (Wikipedia).

is introduced, with the aim to represent satisfactorily the range of spatial variation in the domain of interest, and to reproduce the location and the intensity of the ETMs. The model is then calibrated against the results of the three-dimensional LTVmud model (van Kessel et al., 2011). Finally, the model results are validated against SSC measurements from stations S3 (Buoy 87) to S17 (Wetteren) obtained by filtration of water sampling (Section 4.4).

Sensitivity analyses are undertaken about the values of all the parameters of the sediment module. In order to quantify the goodness of each simulation, different types of error are defined. The temporal error E_t evaluates the error of the model regarding the time series of turbidity measurements from station S1 and S2:

$$E_t = \frac{\sqrt{\sum_t \left((C_{\mathrm{ss}})_{\mathrm{data}} - (C_{\mathrm{ss}})_{\mathrm{model}}\right)^2}}{\sqrt{\sum_t \left((C_{\mathrm{ss}})_{\mathrm{data}}\right)^2}}, \tag{12}$$

where $\sum_t$ means the sum over different times, and C_{ss} is evaluated at a specific point (either station S1 or S2). The spatial error E_x evaluates the error between SLIM and LTVmud along a virtual line that follows the main channel of the estuary:

$$E_x = \frac{\sqrt{\sum_x \left((f)_{\mathrm{LTVmud}} - (f)_{\mathrm{SLIM}}\right)^2 \Delta x}}{\sqrt{\sum_t \left((f)_{\mathrm{LTVmud}}\right)^2 \Delta x}}, \tag{13}$$

where $\sum_x$ means the sum over different positions, Δx is the distance between two points along the virtual line, and f is a function of SSC (either the mean, maximum, or minimum SSC at a specific position).

4.1 Variations at the tidal and spring/neap cycle scales

In order to isolate the variations of the SSC at the tidal and spring/neap cycle scales, the model is first calibrated for a spring/summer situation against turbidity measurements at stations S1 (Terneuzen) and S2 (Baalhoek). Because these fluctuations are following the tidal regime, they should be reproduced rather well only taking into account the hydrodynamics. A set of constant values for the three parameters M, τ_{e} and $w_{\mathrm{s},0}$ should therefore be sufficient to reproduce them satisfactorily. Typical values of the parameters M, τ_{e} and $w_{\mathrm{s},0}$, either measured in situ or used in former modeling studies in the Scheldt, may be found in Wu et al. (2005); Arndt et al. (2007); Mietta et al. (2009); van der Wal et al. (2010); van Kessel et al. (2011). A sensitivity analysis is initiated around those values and the results are summarized in Table 2. The results of simulation a.30 are displayed on Figures 3 and 4.

Figure 3 shows the variations of the SSC at the tidal scale. The mean value and the range of variation are correct, but the fine scale variability

| # | Parameters | | | E_t | |
	τ_e [N m^{-2}]	M [kg m^{-2} s^{-1}]	$w_{s,0}$ [m s^{-1}]	Terneuzen (S1)	Baalhoek (S2)
a.01	0.15	$1 \cdot 10^{-5}$	$1 \cdot 10^{-3}$	1.5905	1.0636
a.02			$2 \cdot 10^{-3}$	0.9023	0.5854
a.03			$5 \cdot 10^{-3}$	0.3945	0.3591
a.04			$1 \cdot 10^{-2}$	0.3654	0.4491
a.05		$2 \cdot 10^{-5}$	$2 \cdot 10^{-3}$	1.6269	1.1979
a.06			$5 \cdot 10^{-3}$	0.7726	0.5956
a.07			$1 \cdot 10^{-2}$	0.4279	0.4556
a.08			$2 \cdot 10^{-2}$	-	-
a.09		$3 \cdot 10^{-5}$	$2 \cdot 10^{-3}$	2.2073	1.7106
a.10			$5 \cdot 10^{-3}$	1.1399	0.9048
a.11			$1 \cdot 10^{-2}$	0.6489	0.6386
a.12			$2 \cdot 10^{-2}$	-	-
a.13	0.2	$1 \cdot 10^{-5}$	$1 \cdot 10^{-3}$	1.2149	0.7624
a.14			$2 \cdot 10^{-3}$	0.6570	0.4085
a.15			$5 \cdot 10^{-3}$	0.3480	0.3822
a.16			$1 \cdot 10^{-2}$	0.4309	0.5139
a.17		$2 \cdot 10^{-5}$	$2 \cdot 10^{-3}$	1.2416	0.8679
a.18			$5 \cdot 10^{-3}$	0.5531	0.4374
a.19			$1 \cdot 10^{-2}$	0.3561	0.4217
a.20			$2 \cdot 10^{-2}$	0.4207	0.5728
a.21		$3 \cdot 10^{-5}$	$2 \cdot 10^{-3}$	1.7203	1.2865
a.22			$5 \cdot 10^{-3}$	0.8326	0.6506
a.23			$1 \cdot 10^{-2}$	0.4634	0.4837
a.24			$2 \cdot 10^{-2}$	0.3732	0.8132
a.25	0.3	$1 \cdot 10^{-5}$	$1 \cdot 10^{-3}$	0.7798	0.4411
a.26			$2 \cdot 10^{-3}$	0.4194	0.3226
a.27			$5 \cdot 10^{-3}$	0.4066	0.4825
a.28			$1 \cdot 10^{-2}$	0.5420	0.6124
a.29		$2 \cdot 10^{-5}$	$2 \cdot 10^{-3}$	0.8002	0.5068
a.30			$5 \cdot 10^{-3}$	0.3786	0.3679
a.31			$1 \cdot 10^{-2}$	0.4025	0.4786
a.32			$2 \cdot 10^{-2}$	0.5313	0.6133
a.33		$3 \cdot 10^{-5}$	$2 \cdot 10^{-3}$	1.1520	0.7944
a.34			$5 \cdot 10^{-3}$	0.5144	0.4184
a.35			$1 \cdot 10^{-2}$	0.3651	0.4262
a.36			$2 \cdot 10^{-2}$	0.4479	0.5782

Table 2: Sensitivity analysis for different values of the parameters M, τ_e and $w_{s,0}$, for a spring/summer 2000 situation; the 20 % smallest errors at each station are emphasized in gray; runs a.08 and 1.12 did not reach the end of the simulation period due to an unstable behavior of the erosion and deposition terms.
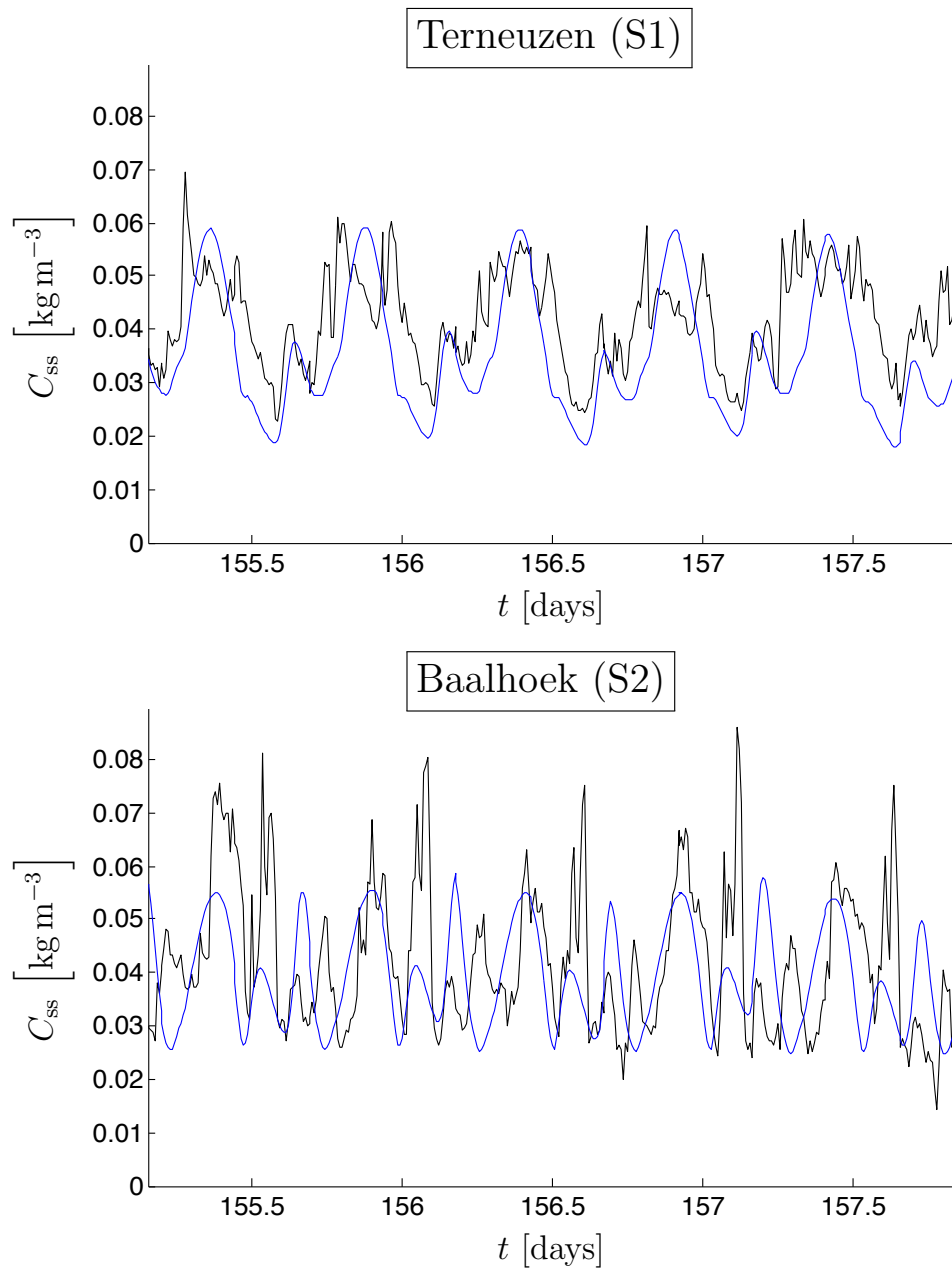
Figure 3: Depth-averaged SSC from 4 July 2000 until 8 July 2000; in black, data deduced from turbidity measurements at different depth levels of stations S1 (Terneuzen) and S2 (Baalhoek); in blue, model results at the same locations, using the set up of simulation a.30 (Table 2).
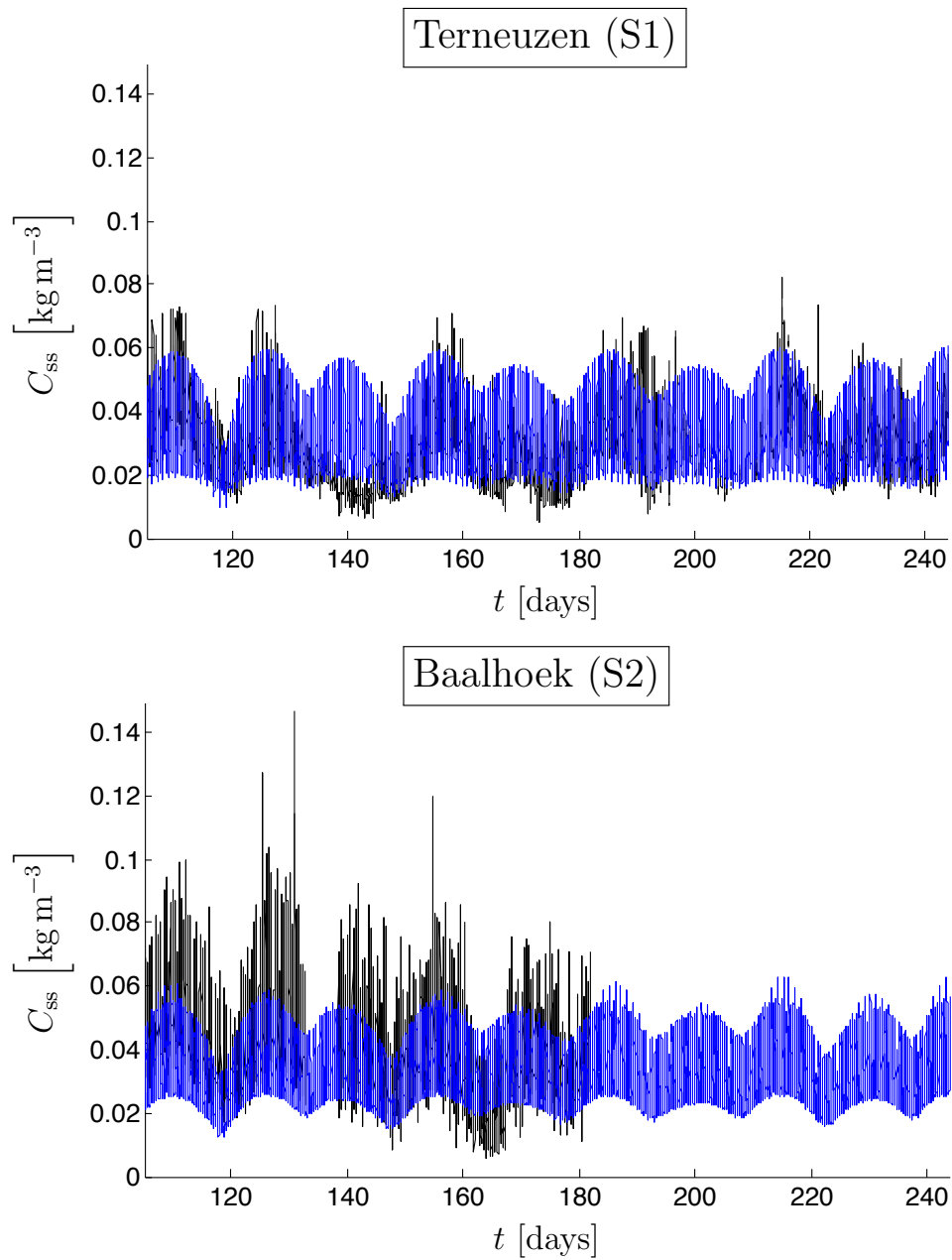
Figure 4: Depth-averaged SSC from 15 April 2000 until 1 September 2000; in black, data deduced from turbidity measurements at different depth levels of stations S1 (Terneuzen) and S2 (Baalhoek); in blue, model results at the same locations, using the set up of simulation a.30 (Table 2).

present in the observations is not reproduced. However, these results obtained with a two-dimensional depth-averaged model are qualitatively comparable to those obtained with more complex three-dimensional models (e.g. van Kessel et al., 2011). Figure 4 displays the variations at the spring/neap cycle scale. The mean value and the range of variation seem correctly represented at Terneuzen. However, they are slightly underestimated at Baalhoek at this stage. Moreover, a set of constant values for the three parameters M, τ_e and $w_{s,0}$ does not allow to represent the seasonal of SSC for simulations over a whole year (not shown). In this form, the model is therefore too simple and additional processes or forcings should be taken into account.

4.2   Variations at the seasonal scale

The observed SSC is significantly higher in winter than in summer. This is not only observed around Terneuzen and Baalhoek (Figure 5), but also along the whole estuary (Fettweis et al., 1998; Chen et al., 2005b; van der Wal et al., 2010). The hydrodynamics exhibits no such variations, at least not in the areas of Terneuzen and Baalhoek, because the tidal discharge in these regions is several hundreds of times higher than the river discharge.

A good candidate to explain this decrease of turbidity in summer is the increase of the biological activity. Indeed, this has been reported to generate a fluffy, interfacial layer on suspended particles that causes them to stick together when colliding (Wolanski, 1995). Therefore, an increase of organic matter concentration in summer implies an increase of floc size that is observed in situ (Maggi, 2009; Mietta et al., 2009). This process is called bioflocculation (Manning et al., 2010) and it suggests that the settling velocity is higher in summer. Moreover, similar processes increase the cohesiveness of muddy bottom sediments in summer which become more difficult to erode (Stolzenbach et al., 1992). This process, called biostabilization (Manning et al., 2010), suggests that the bottom stress threshold value for erosion is also higher in summer (van der Wal et al., 2010).

Although the biological activity is not a variable of the present model and is moreover difficult to quantify, there is a strong correlation between biological activity and water temperature, for which data are available[3]. In the new parametrizations proposed here, the reference settling velocity and the threshold value of the bottom stress for erosion are functions of the water temperature T. The reference settling velocity is equal to its summer value $w_{s,0}^s$, multiplied by a factor decreasing linearly from 1 in summer ($T = T_s$) to $P_T < 1$ in winter ($T = T_w$):

$$w_{s,0} \;\; = \;\; w_{s,0}^s \left((P_T - 1) \frac{T - T_s}{T_w - T_s} + 1 \right), \qquad (14)$$

---

[3]Hydro Meteo Centrum Zeeland, Middelburg, The Netherlands (`www.hmcz.nl`)

where $T_s = 20\,^\circ\mathrm{C}$ and $T_w = 5\,^\circ\mathrm{C}$ are typical values of the Scheldt water temperature in summer and winter, respectively. The threshold value of the bottom stress for erosion is equal to its summer value τ_e^s, multiplied by a factor decreasing linearly from 1 in summer ($T = T_s$) to $Q_T < 1$ in winter ($T = T_w$):

$$\tau_e = \tau_e^s\left((Q_T - 1)\frac{T - T_s}{T_w - T_s} + 1\right). \tag{15}$$

A sensitivity analysis is undertaken around different values of the parameters P_T and Q_T to calibrate the model against the data from Terneuzen and Baalhoek for the whole year 2000. The results are summarized in Table 3. The error in Terneuzen is generally higher, but less sensitive to the influence of water temperature. The results of simulation b.13 are displayed on Figure 5. Those results are then validated against data for the year 1999, using the same parametrizations and the same parameter values as simulation b.13. The error E_t is in this case 0.4310 in Terneuzen and 0.4501 in Baalhoek, i.e. rather similar values to those for the year 2000. The results of the 1999 simulation are displayed on Figure 6.

First of all, it has to be mentioned that the new parametrizations (14) and (15) do not alter the quality of the results about the tidal and spring/neap cycle scale variations in summer and summer 2000. Figure 5 shows that the range of variation is quite satisfactorily represented for the first half of 2000. It is less so for the end of the year, at least for Terneuzen since there are no data available for that period in Baalhoek. Concerning the results of 1999 in Figure 6, the SSC variability is slightly underestimated in the late spring in Baalhoek and significantly more during the whole summer in Terneuzen.

The differences between the model outputs and the data must be explained by processes and forcings that are not taken into account in the model. Among them, the influence of important wind events, which may soften the bottom layer in shallow areas and therefore increase its erodibility, must probably be excluded. Indeed, no significant wind event is reported for the periods when the data are significantly higher than the model results (not shown). On the other hand, dredging events or shipping activities are known to locally have a significant impact on the SSC (Chen et al., 2005b). However, due to data missing on these events, they are very difficult, even impossible, to quantify and to incorporate into the model. On top of those dredging and shipping activities, the area of Terneuzen is influenced by the inputs from the connexion with the Ghent-Terneuzen canal. Finally, another possible cause to explain the seasonal variation of SSC would be the seasonal variation in sediment supply from upstream (due to variations in land erosion and discharges) and downstream (due to variations in the frequency of storms and biological activity). More accurate data at the upstream boundaries and a better calibration of the model into the sea could, therefore, also improve the results.

#	Parameters		E_t	
	P_T	Q_T	Terneuzen (S1)	Baalhoek (S2)
b.01	1	1	0.5605	0.5244
b.02		0.7	0.5033	0.4511
b.03		0.5	0.4565	0.3970
b.04		0.35	0.4232	0.3785
b.05		0.2	0.4366	0.4871
b.06	0.7	1	0.5216	0.4682
b.07		0.7	0.4651	0.3967
b.08		0.5	0.4257	0.3617
b.09		0.35	0.4118	0.3869
b.10		0.2	0.4808	0.5746
b.11	0.5	1	0.4883	0.4144
b.12		0.7	0.4378	0.3547
b.13		0.5	0.4142	0.3571
b.14		0.35	0.4304	0.4425
b.15		0.2	0.5624	0.7140
b.16	0.35	1	0.4602	0.3612
b.17		0.7	0.4249	0.3329
b.18		0.5	0.4299	0.3951
b.19		0.35	0.4881	0.5464
b.20		0.2	0.6900	0.9035
b.21	0.2	1	0.4454	0.3108
b.22		0.7	0.4581	0.3817
b.23		0.5	0.5274	0.5468
b.24		0.35	0.6592	0.7883
b.25		0.2	0.9745	1.2796

Table 3: Sensitivity analysis for different values of the parameters P_T and Q_T, for a full year 2000 situation, with equations (14) and (15), and $M = 2 \cdot 10^{-5}\,\mathrm{kg\,m^{-2}\,s^{-1}}$, $w_{s,0}^s = 5 \cdot 10^{-3}\,\mathrm{m\,s^{-1}}$ and $\tau_e^s = 0.3\,\mathrm{N\,m^{-2}}$; the 20 % smallest errors at each stations are emphasized in gray.
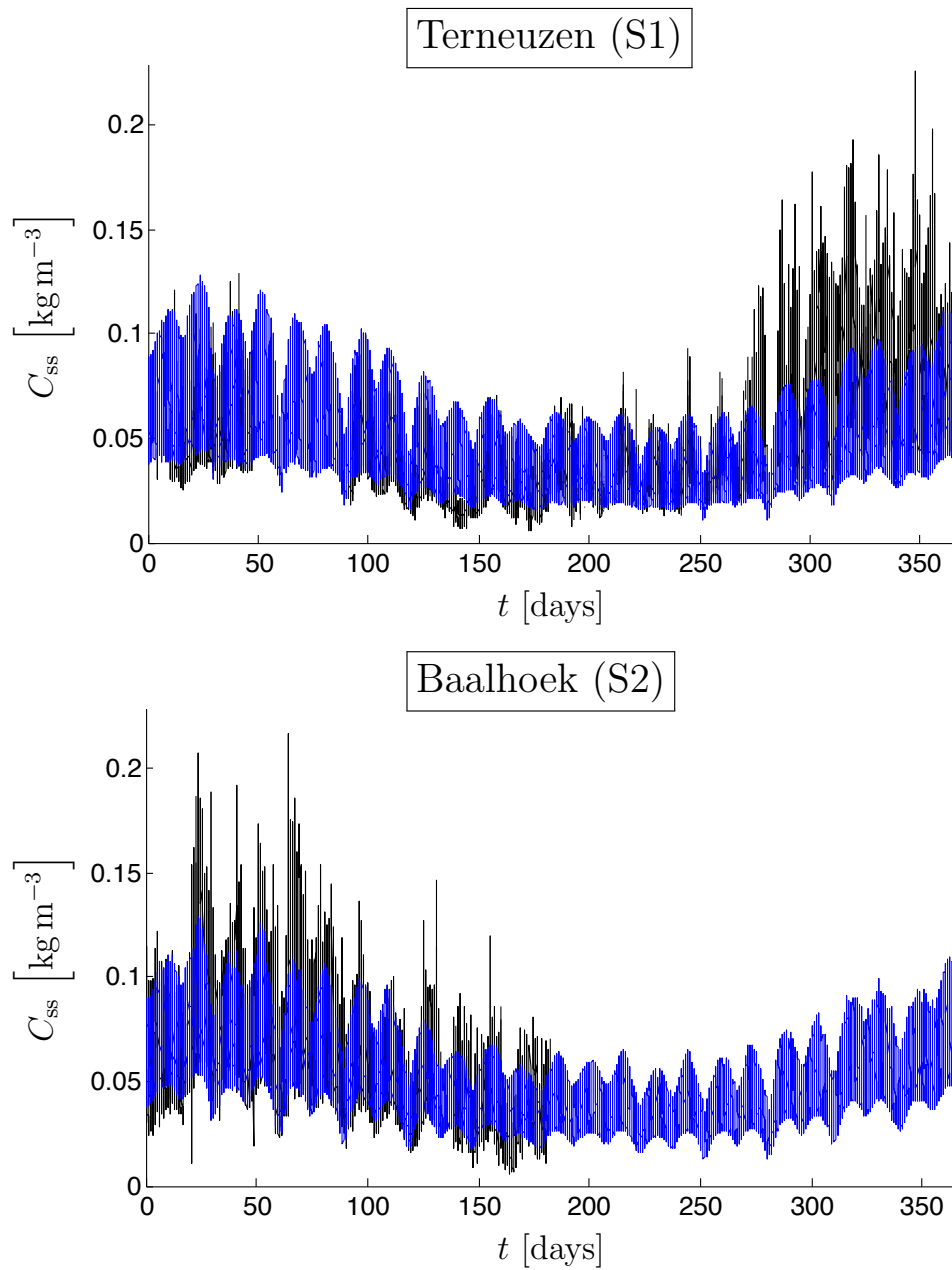
Figure 5: Depth-averaged SSC in 2000; in black, data deduced from turbidity measurements at different depth levels of stations S1 (Terneuzen) and S2 (Baalhoek); in blue, model results at the same locations, using the set up of simulation b.13 (Table 3).
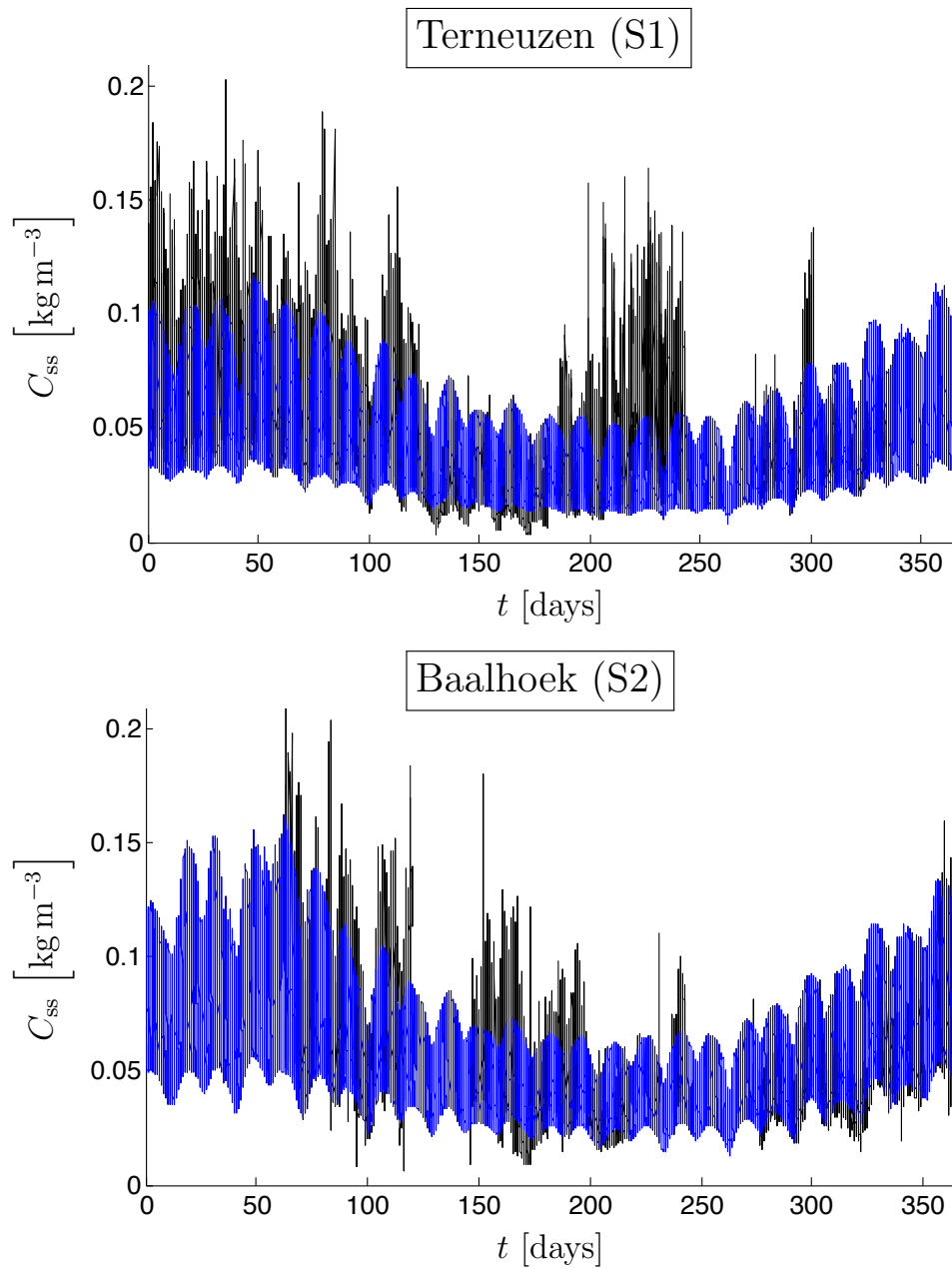
Figure 6: Depth-averaged SSC in 1999; in black, data deduced from turbidity measurements at different depth levels of stations S1 (Terneuzen) and S2 (Baalhoek); in blue, model results at the same locations, using the set up of simulation b.13 (Table 3).

4.3 Different behaviors in Terneuzen and Baalhoek

Section 4.1 and Figure 4 pointed out the distinct behaviors in Terneuzen and Baalhoek. The mean value and the range of SSC variation at the spring/neap cycle scale seemed correctly represented at Terneuzen, but slightly underestimated at Baalhoek. To further improve the simulations, it would therefore be necessary to add a feature which varies in space, e.g. along the estuary axis. Among the main parameters of the sediment module, τ_e is one of the most likely to vary along the estuary. Indeed, the ease of erosion is likely to be related to the bottom sediment composition, which varies in space: sediments composed or containing significant fractions of fine-grained material have greater resistance to entrainment than coarser sediments consisting only of sands (Vanoni, 2006). To take this behavior into account, the parametrization of τ_e may be improved so as to be a function of p, the mud proportion in bottom sediments. To this end, equation (15) is multiplied by a factor increasing linearly from 1 in sandy regions ($p \leq p_s = 0.1$) to $Q_p > 1$ in muddy areas ($p \geq p_m = 0.5$):

$$
\tau_e = \tau_e^{ss}\left((Q_T - 1)\frac{T - T_s}{T_w - T_s} + 1 \right)\left((Q_p - 1)\frac{\hat{p} - p_s}{p_m - p_s} + 1 \right), \quad (16)
$$

where τ_e^{ss} is the summer value of τ_e in sandy regions, and $\hat{p}$ is the mud proportion p bounded to p_s and p_m, so that $p_s \leq \hat{p} \leq p_m$. The data maps used to evaluate the mud proportion p in the estuary are retrieved from extensive campaigns for measuring the sediment composition of the Western Scheldt in 1992 and 1993 (McLaren, 1993).

A sensitivity analysis with respect to different values of the parameters Q_p and τ_e^{ss}. It can be verified that the previous results are not altered with this new parametrization. The mud proportion in Terneuzen and Baalhoek are indeed rather different, but the results summarized in Table 4 show errors of the same order of magnitude, compared to Table 3. In particular, simulation c.04 presents errors very similar to the best previous ones. On the other hand, this new parametrization solves the problem observed in Section 4.1. The mean value, and, to a lesser degree, the range of variation of SSC at the spring/neap cycle scale seemed now improved at both stations (Figure 7).

4.4 Longitudinal profile and ETMs

So far, the model is calibrated using data from two measurement stations (S1 and S2) that are located downstream of the main ETM (Figure 1). In this section, the aim is to assess the behavior of the model around and upstream of the main ETM. To this end, the model is calibrated against depth-averaged outputs from the more complex three-dimensional LTVmud model (van Kessel et al., 2011) during the autumn 2006, and then validated

#	Parameters		E_t	
	Q_p	$\tau_{\mathrm{e}}^{\mathrm{ss}}$ [N m^{-2}]	Terneuzen (S1)	Baalhoek (S2)
c.01	2	0.5	0.5796	0.4335
c.02		0.4	0.5278	0.3784
c.03		0.3	0.4678	0.3522
c.04		0.25	0.4402	0.3783
c.05		0.2	0.4272	0.4597
c.06		0.15	0.4613	0.6303
c.07		0.1	0.6226	0.9653
c.08	3	0.5	0.6149	0.4543
c.09		0.4	0.5660	0.3965
c.10		0.3	0.5051	0.3578
c.11		0.25	0.4718	0.3708
c.12		0.2	0.4432	0.4352
c.13		0.15	0.4412	0.5870
c.14		0.1	0.5361	0.8987
c.15	5	0.3	0.5480	0.3691
c.16		0.25	0.5134	0.3692
c.17		0.2	0.4767	0.4148
c.18		0.15	0.4486	0.5443
c.19		0.1	0.4775	0.8296

Table 4: Sensitivity analysis for different values of the parameters Q_p and $\tau_{\mathrm{e}}^{\mathrm{s}}$, for a full year 2000 situation, with equations (14) and (16), and $M = 2 \cdot 10^{-5}\,\mathrm{kg\,m^{-2}\,s^{-1}}$, $w_{\mathrm{s},0}^{\mathrm{s}} = 5 \cdot 10^{-3}\,\mathrm{m\,s^{-1}}$, $P_T = 0.5$ and $Q_T = 0.5$; the 20 % smallest errors at each stations are emphasized in gray.
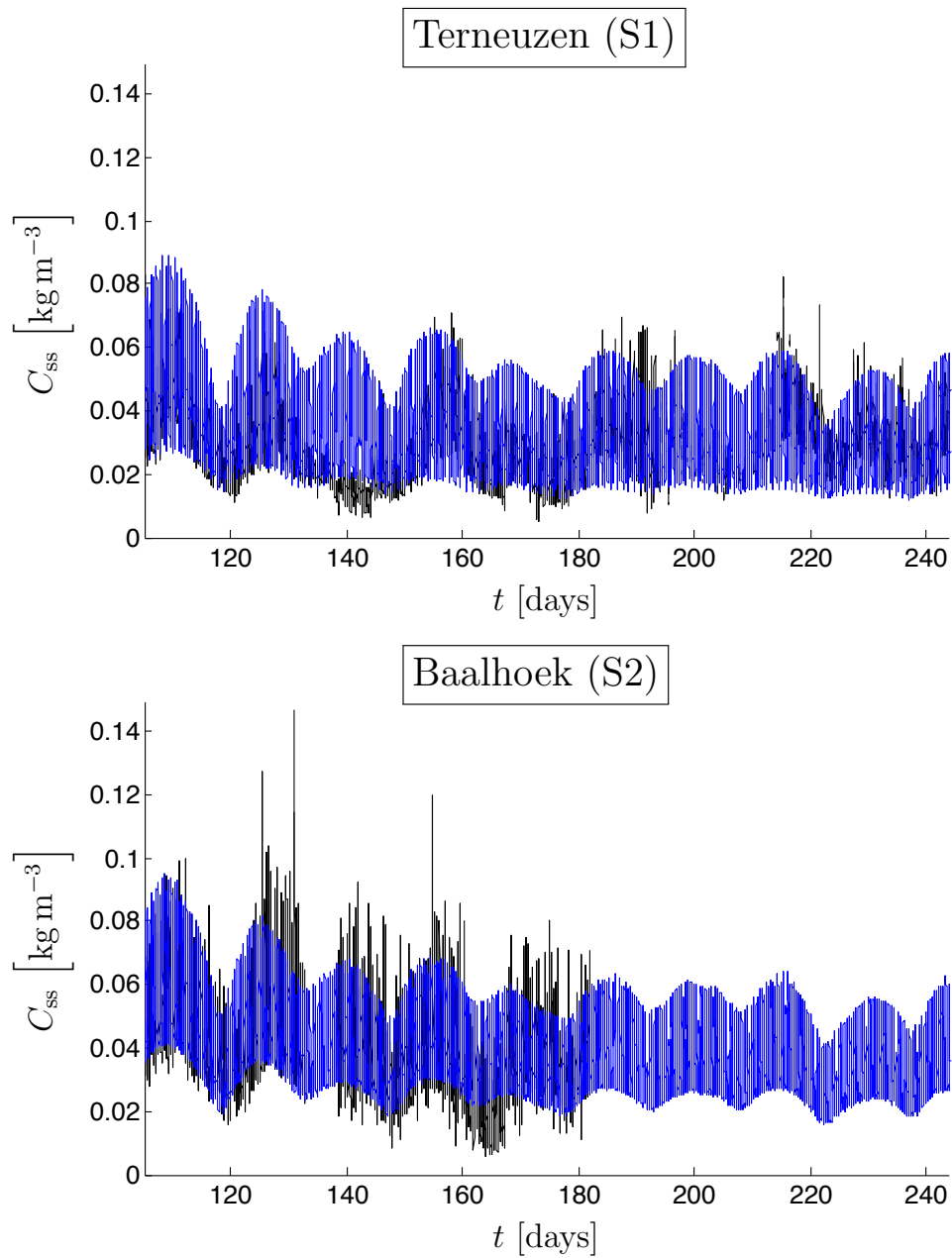
Figure 7: Depth-averaged SSC from 15 April 2000 until 1 September 2000; in black, data deduced from turbidity measurements at different depth levels of stations S1 (Terneuzen) and S2 (Baalhoek); in blue, model results at the same locations, using the set up of simulation c.04 (Table 4).

against monthly SSC measurements performed during the whole year 2002 along the Belgian part of the Scheldt Estuary and River. In this section, the results are presented along a virtual line that follows the main channel of the estuary, from the sea (km 0) to Ghent (km 160).

As it is defined so far, the model is more or less able to represent the location of the main ETM in the correct area. However, comparing with observations in Chen et al. (2005b) and Arndt et al. (2007), with the measurements of 2002, or with the outputs from the LTVmud model, the SSC is largely underestimated around and upstream of the main ETM (not shown). Once again, it is necessary to add a feature which varies along the estuary axis. The parametrization of τ_e has been enriched in Section 4.3 to take into account the influence of the bottom sediment composition. Unfortunately, the consequence of this new parametrization is an increase of τ_e is the region around and upstream of the main ETM, where the bottom sediments are rather muddy. Therefore, this does not solve the problem of underestimated SSC in this part of the domain (not shown). However, $w_{s,0}$ is another parameter that is likely to vary along the estuary.

Several factors may imply lower values of the settling velocity, and therefore higher SSC, around and upstream of the main ETM. Besides the influence of SSC, turbulence and shear stress that are already taken into account through equation (11), salinity is also a factor that influences the flocculation processes (Xia et al., 2004; Chen, 2009). It has the effect to increase the ability of suspended sediment particles to aggregate (van Leussen, 1999; Mietta et al., 2009), so that the settling velocity is lower in fresh waters. However, the transition zone of this phenomenon is rather small and is limited to the upstream part of the salinity intrusion, where the water becomes brackish ($0 \leq S \leq S_{\max}$). To consider this phenomenon, the parametrization of $w_{s,0}$ must be modified so as to be a function of the salinity S, but only within the transition range. To that end, equation (14) is multiplied by a factor decreasing linearly from 1 in salty and brackish waters ($S \geq S_{\max}$) to $P_S < 1$ in fresh waters ($S = 0$):

$$w_{s,0} = w_{s,0}^{\mathrm{sf}}\left((P_T - 1)\frac{T - T_{\mathrm{s}}}{T_{\mathrm{w}} - T_{\mathrm{s}}} + 1 \right)\left((P_S - 1)\frac{S_{\max} - \hat{S}}{S_{\max}} + 1 \right), \quad (17)$$

where $\hat{S}$ is the salinity S bounded to $S_{\max}$, so that $0 \leq \hat{S} \leq S_{\max}$, and $S_{\max} = 6$. Several simulations are carried out with different values of the parameter P_S. The results are summarized in Table 5. The results have indeed improved using the refined parametrization of $w_{s,0}$, with a optimal value of P_S around 0.1. However, the improvements are mostly located in the region upstream of the main ETM, not in the ETM itself (not shown).

The location of the main ETM corresponds more or less to a zone of convergence of the saline upstream directed bottom current and the downstream directed river flow, both carrying fine material (Baeyens et al., 1998b;

25

#	Parameter	E_x		
	P_S	mean	max.	min.
d.01	1	0.6783	0.7259	0.8642
d.02	0.7	0.6306	0.6951	0.8260
d.03	0.5	0.5787	0.6623	0.7806
d.04	0.35	0.5166	0.6240	0.7215
d.05	0.2	0.4101	0.5578	0.6044
d.06	0.15	0.3605	0.5231	0.5364
d.07	0.1	0.3280	0.4808	0.4452
d.08	0.07	0.3743	0.4602	0.3947
d.09	0.05	0.4939	0.4671	0.4251

Table 5: Sensitivity analysis for different values of the parameter P_S, for an autumn 2006 situation, with equations (16) and (17), and $M = 2 \cdot 10^{-5}\,\mathrm{kg\,m^{-2}\,s^{-1}}$, $\tau_e^{ss} = 0.25\,\mathrm{N\,m^{-1}}$, $Q_T = 0.5$, $Q_p = 2$, $w_{s,0}^{sf} = 5 \cdot 10^{-3}\,\mathrm{m\,s^{-1}}$ and $P_T = 0.5$; the 20 % smallest errors for each function are emphasized in gray.

Verlaan et al., 1998). Sometimes, even a non-compacted, mobile fluid mud layer can form. Obviously, the actual 3D processes cannot be represented by a 2D depth-averaged model. but the presence of a fluid mud layer could be parametrized by locally increasing the erosion rate parameter M. Therefore, the parametrization of M is modified by appending a factor increasing as a gaussian from 1 outside the convergence zone to $R_s > 1$ in its center:

$$M = M_0\Big(\big(R_s - 1\big)\exp\Big(-\big(s-\mu\big)^2/2\sigma^2\Big) + 1\Big), \qquad (18)$$

where M_0 is the value of the erosion rate parameter outside the convergence zone, s is the curvilinear coordinate along the longitudinal profile (it is equal to 0 at the mouth), μ is the position of the convergence zone center and σ defines its width.

According to the shape of the main ETM, μ and σ are fixed to 90 km and 10 km, respectively. A sensitivity analysis is undertaken using different combinations of value for the parameters R_s and P_S, the results of which are summarized in Table 6. With this new parametrization of M, the error on the mean SSC, but above all the error on the maximum and minimum SSC have decreased. The best results seem to be obtained for $R_s = 5$ and $P_S = 0.1$. It is even more true if the center of the "convergence zone" (i.e. where M is increased) is moved 5 km downstream (Table 7). The results of simulation f.07 are displayed on Figure 8. This run is considered as the best one and establishes the final set up of this calibration study. The range of variation of the three main parameters, i.e. M, τ_e and $w_{s,0}$ are gathered in Table 8.

In Figure 8, the main ETM is clearly apparent in the mean and maximum SSC values from both models (approximately from km 70 to km 120) and its

#	Parameters		E_x		
	R_s	P_S	mean	max.	min.
e.01	2	1	0.6525	0.6994	0.8570
e.02		0.7	0.6011	0.6652	0.8171
e.03		0.5	0.5454	0.6289	0.7968
e.04		0.35	0.4787	0.5869	0.7082
e.05		0.2	0.3652	0.5167	0.5858
e.06		0.15	0.3145	0.4818	0.5132
e.07		0.1	0.2924	0.4400	0.4117
e.08		0.07	0.3614	0.4237	0.3617
e.09		0.05	0.5012	0.4400	0.4015
e.10	3	1	0.6338	0.6790	0.8522
e.11		0.7	0.5802	0.6422	0.8112
e.12		0.5	0.5223	0.6042	0.7629
e.13		0.35	0.4536	0.5597	0.6997
e.14		0.2	0.3393	0.4871	0.5739
e.15		0.15	0.2926	0.4523	0.4993
e.16		0.1	0.2879	0.4157	0.3947
e.17		0.07	0.3770	0.4098	0.3456
e.18		0.05	0.5311	0.4423	0.3952
e.19	5	1	0.6076	0.6488	0.8456
e.20		0.7	0.5518	0.6091	0.8032
e.21		0.5	0.4926	0.5692	0.7535
e.22		0.35	0.4243	0.5248	0.6884
e.23		0.2	0.3217	0.4569	0.5590
e.24		0.15	0.2930	0.4300	0.4824
e.25		0.1	0.3276	0.4154	0.3767
e.26		0.07	0.4443	0.4408	0.3322
e.27		0.05	0.6140	0.5105	0.3964
e.28	7	1	0.5898	0.6272	0.8408
e.29		0.7	0.5340	0.5868	0.7978
e.30		0.5	0.4762	0.5474	0.7471
e.31		0.35	0.4126	0.5063	0.6808
e.32		0.2	0.3325	0.4524	0.5496
e.33		0.15	0.3262	0.4400	0.4726
e.34		0.1	0.3930	0.4548	0.3679
e.35		0.07	0.5266	0.5113	0.3292
e.36		0.05	0.7061	0.6102	0.4016
e.37	10	1	0.5727	0.6046	0.8362
e.38		0.7	0.5193	0.5655	0.7918
e.39		0.5	0.4669	0.5301	0.7400
e.40		0.35	0.4153	0.4982	0.6725
e.41		0.2	0.3757	0.4753	0.5402
e.42		0.15	0.3986	0.4871	0.4632
e.43		0.1	0.4994	0.5442	0.3611
e.44		0.07	0.6512	0.6386	0.3300
e.45		0.05	0.8428	0.7695	0.4123

Table 6: Sensitivity analysis for different values of the parameters R_s and P_S, for an autumn 2006 situation, with equations (16), (17) and (18), and $\tau_e^{ss} = 0.25\,\mathrm{N\,m^{-1}}$, $Q_T = 0.5$, $Q_p = 2$, $w_{s,0}^{sf} = 5 \cdot 10^{-3}\,\mathrm{m\,s^{-1}}$, $P_T = 0.5$, $M_0 = 2 \cdot 10^{-5}\,\mathrm{kg\,m^{-2}\,s^{-1}}$, $\mu = 90\,\mathrm{km}$ and $\sigma = 10\,\mathrm{km}$; the 20 % smallest errors for each function are emphasized in gray.

#	Parameters	E_x		
	P_S	mean	max.	min.
f.01	1	0.6134	0.6523	0.8478
f.02	0.7	0.5580	0.6134	0.8060
f.03	0.5	0.4984	0.5736	0.7566
f.04	0.35	0.4280	0.5290	0.6922
f.05	0.2	0.3131	0.4577	0.5638
f.06	0.15	0.2700	0.4253	0.4875
f.07	0.1	0.2808	0.3868	0.3801
f.08	0.07	0.3857	0.4038	0.3296
f.09	0.05	0.5495	0.4526	0.3843

Table 7: Sensitivity analysis for different values of the parameter P_S, for an autumn 2006 situation, with equations (16), (17) and (18), and $\tau_e^{ss} = 0.25\,\mathrm{N\,m^{-1}}$, $Q_T = 0.5$, $Q_p = 2$, $w_{s,0}^{sf} = 5 \cdot 10^{-3}\,\mathrm{m\,s^{-1}}$, $P_T = 0.5$, $M_0 = 2 \cdot 10^{-5}\,\mathrm{kg\,m^{-2}\,s^{-1}}$, $R_s = 5$, $\mu = 85\,\mathrm{km}$ and $\sigma = 10\,\mathrm{km}$; the 20 % smallest errors for each function are emphasized in gray.
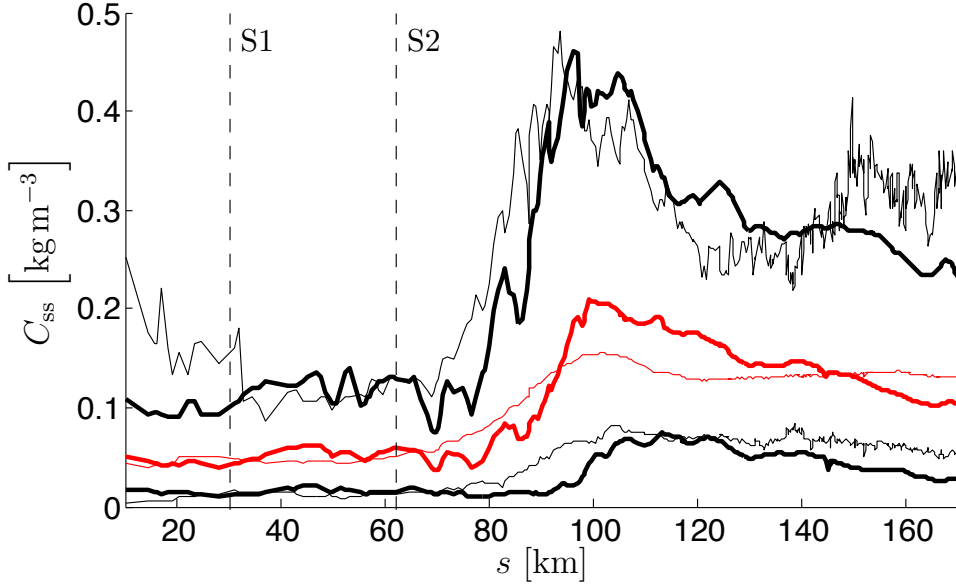
Figure 8: Longitudinal profile of mean (red), maximum and minimum (black) SSC between October 1, 2006 and December 31, 2006, from the mouth (km 0) to Ghent (km 180); thick lines are model results obtained using the set up of simulation f.07 (Table 7); thin lines are results from the three-dimensional LTVmud model (van Kessel et al., 2011).

	min.	max.
M $[\mathrm{kg\,m^{-2}\,s^{-1}}]$	2×10^{-5}	1×10^{-4}
τ_e $[\mathrm{N\,m^{-2}}]$	0.125	0.5
$w_\mathrm{s,0}$ $[\mathrm{m\,s^{-1}}]$	2.5×10^{-4}	5×10^{-3}

Table 8: Range of variation of the three main parameters of the sediment module, using the set up of simulation f.07 (Table 7).

intensity is in accordance with the observations in Chen et al. (2005b) and Arndt et al. (2007). In the river part (i.e. km 100-170), the models have more different behaviors. The LTVmud model maximum values are almost as high in the river ETM as in the main ETM. But still, even if the model described in this paper does not feature a clear local maximum, both the maximum or the mean values of the SSC are higher in the river part than downstream of the main ETM. This can be identified as the river ETM. Anyway, the consistency between the results from both models is remarkable.

In Figure 9, the model results are presented for year 2002, against the measurement data sampled at that period. Looking at the mean and maximum values of the SSC, the main ETM is again clearly apparent and with the expected intensity. Moreover, the range is well reproduced almost all along the estuary, as only a few data are found outside the range of the model values.

5   Summary and conclusion

The objective of this study was to design a sediment module for the two-dimensional depth-averaged and one-dimensional section-averaged components of SLIM, in order to represent satisfactorily the main features of the SSC dynamics in the Scheldt Estuary and tidal river network. The initial idea was to develop a module as simple as possible, with only three parameters: M the erosion rate parameter, τ_e the bottom stress threshold value for erosion, and w_s the settling velocity. However, to be able to represent accurately the variations of the SSC at timescales ranging from hours to a year at two locations in the estuary, improved parametrizations proved to be necessary.

For example, the influence of biological activity appeared crucial to model accurately the seasonal variations of the SSC. First because of its influence on the flocculation processes, along with the SSC itself, the turbulence or the shear stress, increasing the settling velocity w_s in summer. But also because it has an impact on the erodibility of the bottom sediments, increasing τ_e in summer.

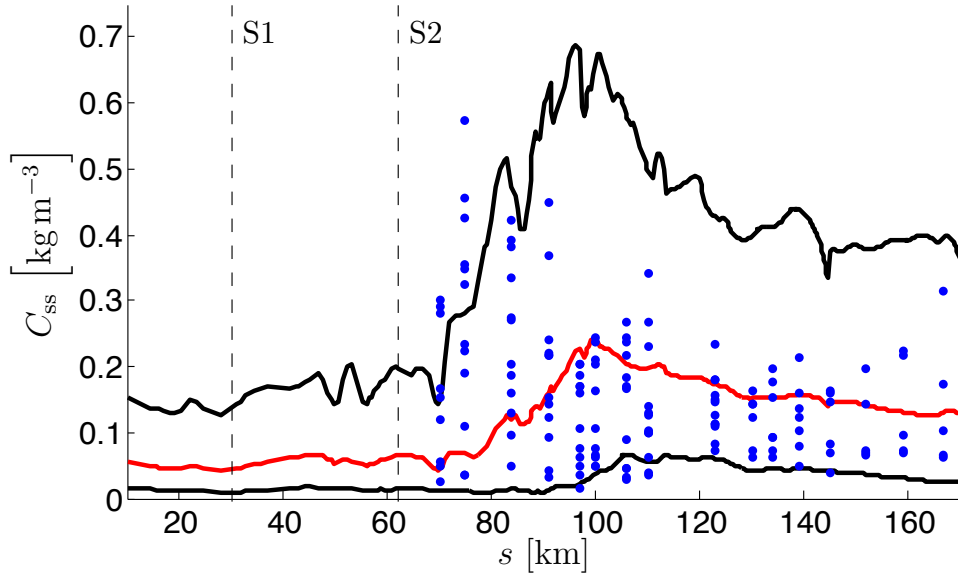With those improvements, the model produced an ETM in the area

Figure 9: Longitudinal profile of mean (red), maximum and minimum (black) SSC during year 2002, from the mouth (km 0) to Ghent (km 180); model results obtained using the set up of simulation f.07 (Table 7); in blue, monthly SSC measurements at stations S3 to S17 (Figure 1).

of Antwerp, but its intensity was too small and the river ETM was not present. The influence of salinity on the flocculation processes (salinity acts as a gluey agent on suspended sediments) make the river ETM appear. For a realistic reproduction of the main ETM, the parametrization of M has been enriched to consider the influence of a convergence zone between bottom currents carrying large amounts of fine sediments.

The parametrizations proposed in Section 4 are empirical rather than physical, but this is justified by the applied nature of the study. Besides, this strategy allowed to identify what seems to be the key processes governing the sediment dynamics in the Scheldt Estuary. And the depth-averaged two-dimensional sediment model presented herein, with only one type of sediments, proved to be able to represent rather satisfactorily the main features of the SSC dynamics in the Scheldt Estuary and tidal river, i.e.

- the order of magnitude of the SSC throughout the estuary and the tidal river network;

- the variations of the SSC at the tidal, spring/neap cycle and seasonal timescales;

- the locations of the main ETM and the river ETM.

This is an important result by itself. Environmental studies may indeed

30

require relatively long simulations compared to some short-term processes of the sediment dynamics. The computer cost for such simulations may be too high when using modern three-dimensional models, but this is less so using the model presented in this paper.

Acknowledgements

A One-dimensional equations

The one-dimensional equations used in the riverine part of the domain are

$$\frac{\partial A}{\partial t} + \frac{\partial}{\partial x}(Au) = 0, \tag{19}$$

$$\frac{\partial u}{\partial t} + u\frac{\partial u}{\partial x} + g\frac{\partial \eta}{\partial x} = \frac{1}{A}\frac{\partial}{\partial x}\left(A\nu\frac{\partial u}{\partial x}\right) - \frac{\tau_{\mathrm{b}}}{\rho H}, \tag{20}$$

$$\frac{\partial(AS)}{\partial t} + \frac{\partial}{\partial x}(AuS) = \frac{\partial}{\partial x}\left(A\kappa\frac{\partial S}{\partial x}\right), \tag{21}$$

$$\frac{\partial(AC_{\mathrm{ss}})}{\partial t} + \frac{\partial}{\partial x}(AuC_{\mathrm{ss}}) = \frac{\partial}{\partial x}\left(A\kappa\frac{\partial C_{\mathrm{ss}}}{\partial x}\right) + b(E_{\mathrm{p}} + E_{\mathrm{f}} - D), \tag{22}$$

$$\frac{\partial(bC_{\mathrm{sb}})}{\partial t} = b(D - E_{\mathrm{f}}), \tag{23}$$

where t is the elapsed time and x is the along-river coordinate. The dependent variable of the continuity equation (19) is the cross-section area A [m^2]. The dependent variable of the momentum conservation equation (20) is the section-averaged longitudinal velocity [m s^{-1}], and the effective water depth is computed as follows

$$H = \frac{A}{b}, \tag{24}$$

where b [m] is the river width:

$$b = \frac{\partial A}{\partial \eta}. \tag{25}$$

River widths and sections data for different values of the local elevation are given as topological inputs of the model (de Brye et al., 2010). The variables of the tracer equations (21) to (23) are the same as in the two-dimensional model, except that they are here averaged over the section (S and C_{ss}) or the bottom width (C_{sb}). The parametrizations are exactly the same.

The equations (19) to (23) are solved using SLIM and and a discontinuous Galerkin discretization with linear shape functions for every variable. The temporal integration is performed the same way as in the two-dimensional component and the vertical exchange processes of the sediment equations are also solved as pointwise ordinary differential equations.

References

Arndt, S., Vanderborght, J.-P., and Regnier, P. (2007). Diatom growth response to physical forcing in a macrotidal estuary: Coupling hydrodynamics, sediment transport, and biogeochemistry. *Journal of Geophysical Research*, 112:C05045, doi:10.1029/2006JC003581.

Baeye, M., Fettweis, M., Voulgaris, G., and Van Lancker, V. (2011). Sediment mobility in response to tidal and wind-driven flows along the belgian inner shelf, southern North Sea. *Ocean Dynamics*, 61:611–622, doi:10.1007/s10236-010-0370-7.

Baeyens, W., Elskens, M., Gillain, G., and Goeyens, L. (1998a). Biogeochemical behaviour of Cd, Cu, Pb and Zn in the Scheldt estuary during the period 1981-1983. *Hydrobiologia*, 366:15–44, doi:10.1023/A:1003168125869.

Baeyens, W., van Eck, B., Lambert, C., Wollast, R., and Goeyens, L. (1998b). General description of the Scheldt estuary. *Hydrobiologia*, 366:1–14, doi:10.1023/A:1003164009031.

Baugh, J. V. and Manning, A. J. (2007). An assesment of a new settling velocity parametrisation for cohesive sediment transport modeling. *Continental Shelf Research*, 27:1835–1855.

Berlamont, J., Ockenden, M., Toorman, E., and Winterwerp, J. (1993). The characterisation of cohesive sediment properties. *Coastal Engineering*, 21:105–128, doi:10.1016/0378-3839(93)90047-C.

Blaise, S., de Brye, B., de Brauwere, A., Deleersnijder, E., Delhez, E. J. M., and Comblen, R. (2010). Capturing the residence time boundary layer - application to the Scheldt Estuary. *Ocean Dynamics*, 60:535–554, doi:10.1007/s10236-010-0272-8.

Chen, M. S. (2009). Particle flocculation and distribution in estuarine environment. In *Proceedings of the 33rd IAHR Congress, Water engineering for a sustainable environment*, Vancouver, BC, Canada, pages 5030–5037. International Association of Hydraulic Engineering and Research, ISBN:978-90-78046-08-0.

Chen, M. S. and Wartel, S. (2009). Estuarine hydrodynamics and energy. In Tan, S. K. and Huang, Z., editors, *Proceedings of the 5th international Conference on Asian and Pacific coasts*, Singapore, volume 1, pages 216–222. doi:10.1142/9789814287951_0025.

Chen, M. S., Wartel, S., and Temmerman, S. (2005a). Seasonal variation of floc characteristics on tidal flats, the Scheldt estuary. *Hydrobiologia*, 540:181–195, doi:10.1007/s10750-004-7143-6.

Chen, M. S., Wartel, S., van Eck, B., and van Maldegem, D. (2005b). Suspended matter in the Scheldt estuary. *Hydrobiologia*, 540:79–104, doi:10.1007/s10750-004-7122-y.

Comblen, R., Lambrechts, J., Remacle, J.-F., and Legat, V. (2010). Practical evaluation of five partly discontinuous finite element pairs for the non-conservative shallow water equations. *International Journal for Numerical Methods in Fluids*, 63:701–724, doi:10.1002/fld.2094.

de Brauwere, A., de Brye, B., Blaise, S., and Deleersnijder, E. (2011a). Residence time, exposure time and connectivity in the Scheldt Estuary. *Journal of Marine Systems*, 84:85–95, doi:10.1016/j.jmarsys.2010.10.001.

de Brauwere, A., de Brye, B., Servais, P., Passerat, J., and Deleersnijder, E. (2011b). Modelling *Escherichia coli* concentrations in the tidal Scheldt river and estuary. *Water Research*, 45:2724–2738, doi:10.1016/j.watres.2011.02.003.

de Brauwere, A., Gourgue, O., de Brye, B., Servais, P., Ouattara, N. K., and Deleersnijder, E. (2013). Modelling *Escherichia coli* dynamics in the Scheldt land-sea continuum. Part II. The tidal Scheldt River and Estuary. *Journal of Marine Systems*, submitted.

de Brye, B., de Brauwere, A., Gourgue, O., Delhez, E. J. M., and Deleersnijder, E. (2012). Water renewal timescales in the Scheldt Estuary. *Journal of Marine Systems*, 94:74–86, doi:10.1016/j.jmarsys.2011.10.013.

de Brye, B., de Brauwere, A., Gourgue, O., Kärnä, T., Lambrechts, J., Comblen, R., and Deleersnijder, E. (2010). A finite-element, multi-scale model of the Scheldt tributaries, river, estuary and ROFI. *Coastal Engineering*, 57:850–863, doi:10.1016/j.coastaleng.2010.04.001.

Delhez, E. J. M. and Wolk, F. (2012). Diagnosis of the transport of adsorbed material in the Scheldt estuary: a proof of concept. *Journal of Marine Systems*, in press, doi:10.1016/j.jmarsys.2012.01.007.

Dyer, K. R. (1989). Sediment processes in estuaries: future research requirements. *Journal of Geophysical Research*, 94(C10):14327–14339, doi:10.1029/JC094iC10p14327.

Einstein, H. A. and Krone, R. B. (1962). Experiments to determine modes of cohesive sediment transport in salt water. *Journal of Geophysical Research*, 67:1451–1461, doi:10.1029/JZ067i004p01451.

Eisma, D. and Kalf, J. (1979). Distribution and particle size of suspended matter in the Southern Bight of the North sea and the Eastern channel. *Netherlands Journal of Sea Research*, 13:298–324, doi:10.1016/0077-7579(79)90008-5.

Fettweis, M., Sas, M., and Monbaliu, J. (1998). Seasonal, neap-string and tidal variation of cohesive sediment concentration in the Scheldt

Estuary, Belgium. *Estuarine, Coastal and Shelf Science*, 47:21–36, doi:10.1006/ecss.1998.0338.

Fettweis, M. and Van den Eynde, D. (2003). The mud deposits and the high turbidity in the Belgian-Dutch coastal zone, southern bight of the North Sea. *Continental Shelf Research*, 23:669–691, doi:10.1016/S0278-4343(03)00027-X.

Kärnä, T., de Brye, B., Gourgue, O., Lambrechts, J., Comblen, R., Legat, V., and Deleersnijder, E. (2011). A fully implicit wetting-drying method for DG-FEM shallow water models, with an application to the Scheldt Estuary. *Computer Methods in Applied Mechanics and Engineering*, 200:509–524, doi:10.1016/j.cma.2010.07.001.

Maggi, F. (2009). Biological flocculation of suspended particles in nutrient-rich aqueous ecosystems. *Journal of Hydrology*, 376:116–125, doi:10.1016/j.jhydrol.2009.07.040.

Manning, A. J., Langston, W. J., and Jonas, P. J. C. (2010). A review of sediment dynamics in the Severn Estuary: influence of flocculation. *Marine Pollution Bulletin*, 61:37–51, doi:10.1016/j.marpolbul.2009.12.012.

McLaren (1993). Patterns of sediment transport in the western part of the westerschelde. Technical report, GeoSea Consulting, Cambridge, United Kingdom.

Meire, P., Ysebaert, T., Van Damme, S., Van den Bergh, E., Maris, T., and Struyf, E. (2005). The Scheldt estuary: a description of a changing ecosystem. *Hydrobiologia*, 540:1–11, doi:10.1007/s10750-005-0896-8.

Mietta, F., Chassagne, C., Manning, A. J., and Winterwerp, J. C. (2009). Influence of shear rate, organic matter content, pH and salinity on mud flocculation. *Ocean Dynamics*, 59:751–763, doi:10.1007/s10236-009-0231-4.

Okubo, A. (1971). Oceanic diffusion diagrams. *Deep-Sea Research*, 18:789–802, doi:10.1016/0011-7471(71)90046-5.

Ouattara, N. K., Servais, P., and de Brauwere, A. (2011). Modelling *Escherichia coli* dynamics in the Scheldt land-sea continuum. Part I. the drainage network. *Journal of Marine Systems*, in press, doi:10.1016/j.jmarsys.2012.05.004.

Partheniades, E. (1965). Erosion and deposition of cohesive soils. *Journal of the Hydraulics Division*, 91:105–139.

Pejrup, M. and Mikkelsen, O. (2010). Factors controlling the field settling velocity of cohesive sediment in estuaries. *Estuarine, Coastal and Shelf Science*, 87:177–185, doi:10.1016/j.ecss.2009.09.028.

Smagorinsky, J. (1963). General circulation experiments with the primitive equations. I. The basic experiments. *Monthly Weather Review*, 91:99–164.

Soetaert, K. and Herman, P. M. J. (1995). Estimating estuarine residence time in the Westerschelde (The Netherlands) using a box model with fixed dispersion coefficients. *Hydrobiologia*, 311:215–224, doi:10.1007/BF00008582.

Soetaert, K., Middelburg, J. J., Heip, C., Meire, P., Van Damme, S., and Maris, T. (2006). Long-term change in dissolved inorganic nutrients in the heterotrophic Scheldt estuary (Belgium, The Netherlands). *Limnology and Oceanography*, 51:409–423, doi:10.4319/lo.2006.51.1_part_2.0409.

Steen, R. J. C. A., van der Vaart, J., Hiep, M., Van Hattum, B., Cofino, W. P., and Brinkman, U. A. T. (2001). Gross fluxes and estuarine behaviour of pesticides in the Scheldt Estuary (1995-1997). *Environmental Pollution*, 115:65–79, doi:10.1016/S0269-7491(01)00085-9.

Stolzenbach, K. D., Newman, K. A., and Wong, C. S. (1992). Aggregation of fine particles at the sediment-water interface. *Journal of Geophysical Research*, 97(C11):17889–17898, doi:10.1029/92JC01827.

Thieu, V., Billen, G., and Garnier, J. (2009). Nutrient transfer in three contrasting NW European watersheds: The Seine, Somme and Scheldt Rivers. A comparative application of the Seneque/Riverstrahler model. *Water Research*, 43:1740–1754, doi:10.1016/j.watres.2009.01.014.

van der Wal, D., van Kessel, T., Eleveld, M. A., and Vanlede, J. (2010). Spatial heterogeneity in estuarine mud dynamics. *Ocean Dynamics*, 60:519–533, doi:10.1007/s10236-010-0271-9.

van Kessel, T., Vanlede, J., and de Kok, J. (2011). Development of a mud transport model for the Scheldt estuary. *Continental Shelf Research*, 31:S165–S181, doi:10.1016/j.csr.2010.12.006.

van Leussen, W. (1999). The variability of settling velocities of suspended fine-grained sediment in the Ems estuary. *Journal of Sea Research*, 41:109–118, doi:10.1016/S1385-1101(98)00046-X.

Vanderborght, J.-P., Folmer, I. M., Aguilera, D. R., Uhrenholdt, T., and Regnier, P. (2007). Reactive-transport modelling of C, N, and O_2 in a river-estuarine-coastal zone system: application to the Scheldt estuary. *Marine Chemistry*, 106:92–110, doi:10.1016/j.marchem.2006.06.006.

Vanoni, V. A., editor (2006). *Sedimentation engineering*. Number 54 in Manuals and Reports on Engineering Practice. American Society of Civil Engineers.

Verlaan, P. A. J., Donze, M., and Kuik, P. (1998). Marine *vs* fluvial suspended matter in the Scheldt Estuary. *Estuarine, Coastal and Shelf Science*, 46:873–883, doi:10.1006/ecss.1999.0599.

Villars, M. T. and Vos, R. J. (1999). RESTWES: remote sensing as a tool for integrated monitoring of the Western Scheldt. WL Delft Hydraulics Report Z2472, Delft Hydraulics.

White, L., Legat, V., and Deleersnijder, E. (2008). Tracer conservation for three-dimensional, finite-element, free-surface, ocean modeling on moving prismatic meshes. *Monthly Weather Review*, 136:420–442, doi:10.1175/2007MWR2137.1.

Winterwerp, J. C. (1998). A simple model for turbulence induced flocculation of cohesive sediment. *Journal of Hydraulic Research*, 36:309–326, doi:10.1080/00221689809498621.

Winterwerp, J. C. (2002). On the flocculation and settling velocity of estuarine mud. *Continental Shelf Research*, 22:1339–1360, doi:10.1016/S0278-4343(02)00010-9.

Wolanski, E. (1995). Transport of sediment in mangrove swamps. *Hydrobiologia*, 295:31–42, doi:10.1007/BF00029108.

Wolanski, E., Gibbs, R. J., Mazda, Y., Mehta, A., and King, B. (1992). The role of turbulence in the settling of mud flocs. *Journal of Coastal Research*, 8:35–46.

Wu, Y., Falconer, R., and Lin, B. (2005). Modelling trace metal concentration distributions in estuarine waters. *Estuarine, Coastal and Shelf Science*, 64:699–709, doi:10.1016/j.ecss.2005.04.005.

Xia, X. M., Li, Y., Yang, H., Wu, C. Y., Sing, T. H., and Pong, H. K. (2004). Observations on the size and settling velocity distributions of suspended sediment in the Pearl River Estuary, China. *Continental Shelf Research*, 24:1809–1826, doi:10.1016/j.csr.2004.06.009.